

# Properties of the tetravalent actinide series in aqueous phase from a microscopic simulation automated engine

Eléonor Acher,<sup>1</sup> Michel Masella,<sup>2</sup> Valérie Vallet,<sup>3</sup> and Florent Réal<sup>3</sup>

<sup>1</sup>CEA, Nuclear Energy Division, Research Department on Mining and fuel Recycling Processes (LILA), BP17171 F-30207 Bagnols-sur-Cèze, France\*

<sup>2</sup>Laboratoire de Biologie Structurale et Radiobiologie,  
Service de Bioénergétique, Biologie Structurale et Mécanismes,

Institut Joliot, CEA Saclay, F-91191 Gif sur Yvette Cedex, France

<sup>3</sup>Univ. Lille, CNRS, UMR 8523 - PhLAM - Physique des Lasers Atomes et Molécules, F-59000 Lille, France

In the context of nuclear fuel recycling and environmental issues, the understanding of the properties of radio-elements with various approaches remains a challenge regarding their dangerousness. Moreover, experimentally, it is imperative to work at sufficiently high concentrations to reach the sensitivities of the analysis tools, which often leads to precipitation for some of them, and stabilizing of specific oxidation states of some actinides remains a challenge, thus making it difficult to extract general trends across the actinide series. Complementary to experiments, modelling can be used to unbiasedly probe the actinide's properties in aquatic environment and offers a predictive tool. We report the first molecular dynamics simulations based on homogeneously built force fields for the whole series of the tetravalent actinides in aqueous phase from Th<sup>IV</sup> to Bk<sup>IV</sup> and including Pu<sup>IV</sup>. The force fields used to model the interactions among the constituents include polarization and charge donation microscopic effects. They are built from an automated iterative quantum *ab initio* based engine, the core element of a future machine learning procedure devoted to generate accurate force fields. The comparison of our simulated hydrated actinide properties to available experimental data show the model robustness and the relevance of our parameter assignment engine. Moreover our simulated structural, dynamical and hydration free energy data show that, apart from Am<sup>IV</sup> and Cm<sup>IV</sup>, the actinides properties change progressively along the series.

The behavior of actinides, An<sup>IV</sup>, in solution is highly relevant for two application fields connected to the nuclear industry : their separation from the spent nuclear fuels [1], and their migration from nuclear waste repositories [2]. However, the radiotoxicity and the complex chemistry of these elements explain the rather scarce availability of experimental data for them, in particular in aqueous phase. If extended X-ray absorption fine structure (EXAFS) technique yields highly accurate An<sup>IV</sup>/water oxygen bond lengths in the series Th<sup>4+</sup>-Bk<sup>4+</sup>, there are still large uncertainties in the experimental An<sup>IV</sup> hydration numbers,  $N_c$ , ranging from eight to thirteen for Th<sup>4+</sup>-Bk<sup>4+</sup> [3–17].

To complement experimental data, research groups either developed empirical theoretical models or performed quantum chemical computations on small An<sup>IV</sup>/ligand clusters. We may quote here the Born-like model (adjusted from geometrical experimental data) of David et al. [18] that yields An<sup>IV</sup> hydration free energy,  $\Delta G_{\text{hyd}}$  values. These values decrease almost regularly along the An<sup>IV</sup> series. In 2003, David et al. [19] revised their approach. They got then very close tendency, at the remarkable exception of Np<sup>IV</sup> whose  $\Delta G_{\text{hyd}}$  value is shifted by more than  $-30 \text{ kcal mol}^{-1}$  compared to the 1986 data. We may also quote the study of Banik et al. [8] who performed quantum calculations on a set of small An<sup>IV</sup> hydrated clusters (with bulk effects accounted for using a polarizable continuum solvent approach). These authors got An–O<sub>water</sub> bond lengths in line with EXAFS data, and they concluded to a decrease of the An<sup>4+</sup> hydration

number from nine to eight, with a turning point at Cm<sup>4+</sup>.

To go beyond static models, molecular dynamic, MD, simulations have also been considered. However their predictive capability relies on the accuracy of the potential energy used to model microscopic interactions. Potential energies computed from quantum chemistry methods are the most relevant to investigate the properties of any kind of microscopic systems. Regarding An<sup>IV</sup>, we may quote MD studies focusing on the hydration process of Th<sup>4+</sup>, U<sup>4+</sup>, and Pu<sup>4+</sup> using density functional theory (DFT) methods [20–24]. However none of the available DFT methods is able to describe accurately both water/water and cation/water interactions, at least when comparing DFT results to those of higher level quantum *ab initio* methods like the Møller-Plesset second-order perturbation theory, MP2, and above [25] (see discussions of Section 1 of the Supplementary Material). As high end quantum methods cannot be still considered to efficiently simulate bulk systems, even when used in hybrid quantum mechanical/molecular modeling schemes [26, 27], molecular modeling approaches based on empirical interaction potentials, force fields, are still the most suited to simulate such systems on significantly long simulation times.

As discussed by earlier authors [25, 28–30], An<sup>IV</sup>/water microscopic interactions result from a complex interplay between mainly large electrostatic, non-additive polarization and charge-donation effects whose relative magnitude is not obvious to quantify. Moreover and as far as we know, most of the water force fields proposed to date

are not able to capture the magnitude of the water/water repulsive interactions in cation first hydration shells, at the exception of the TCPE/2013 one [30]. This explains the difficulty of building well balanced force fields to study the hydration of  $\text{An}^{\text{IV}}$  and thus the very few  $\text{An}^{\text{IV}}$  MD bulk simulations based on force fields reported to date [20, 25, 30–32].

Besides the choice of a physically meaningful functional form for the force field, another critical issue is the strategy to assign force-field parameters. The most promising strategy consists in assigning the parameters to reproduce only quantum data regarding a set of training molecular clusters. These training data sets usually comprise small molecular clusters optimized in gas phase. We already built accordingly sophisticated force fields, hereafter name Gas-Phase Parameter (GP-P), to study the hydration of  $\text{Th}^{\text{IV}}$  and  $\text{Cm}^{\text{III}}$  [25, 32]. However such an approach implicitly assumes that all the features of bulk phase interactions can be captured by investigating gas phase systems. In the particular case of  $\text{U}^{\text{IV}}$ , Atta-Fynn et al. [24] showed using quantum computations cation/water oxygen distances to be shifted by about 0.05 Å from gas phase to aqueous solution. Because of the +4 charge of  $\text{An}^{\text{IV}}$  elements, such a distance shift yields a change in the Coulombic interaction energy between  $\text{An}^{\text{IV}}$  and each water oxygen of its first hydration shell amounting to about 20 k<sub>B</sub>T at ambient conditions. Hence bulk phase cluster structures have to be considered to build accurate force field. We will denote this kind of force-field Bulk-Phase Parameter (BP-P).

The most common parameter fitting process is a single step procedure consisting in best reproducing the properties of a training molecular cluster set. The ongoing increase of the available computational resources yields research groups to propose more and more sophisticated fitting procedures in line with the machine learning philosophy. We may quote here Monte-Carlo sampling approach of Galbis et al. [33], or the statistical learning parametrization procedure of Fracchia et al. [34]. Following the ideas of Galbis et al. [33], we propose here an automated iterative procedure to homogeneously and coherently built a class of BP-P force fields to investigate the hydration properties of the whole  $\text{An}^{\text{IV}}$  series. These force fields are then used to investigate the geometric, temporal and thermodynamics properties of these cations in aqueous solution. For comparison purpose, we also investigated the behavior of the lanthanide element  $\text{Ce}^{\text{IV}}$  that is often considered as a non radioactive surrogate for  $\text{Pu}^{\text{IV}}$  [35].

#### SELF CONSISTENTLY CONVERGED BP-P FORCE FIELDS FOR $\text{An}^{\text{IV}}$

We model  $\text{An}^{\text{IV}}$ /water interactions using the same force-field functional form as in our earlier works devoted

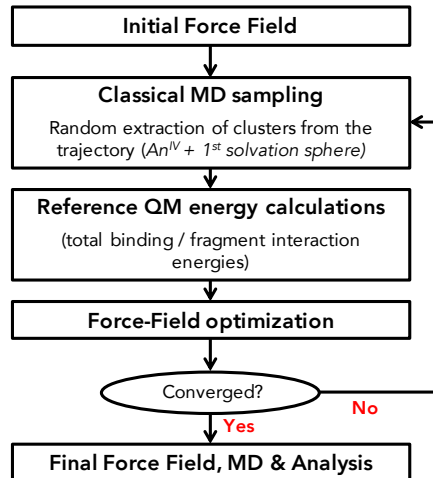


FIG. 1: Chart for the automated iterative parameter optimization procedure. Each MD simulation is at the 10 ns scale. The sampling consists in extracting each 1 ps the  $\text{An}^{\text{IV}}$  plus its first hydration shell clusters. We select then 20 of these clusters whose MM binding energies, BE, corresponding to the reaction  $\text{An}^{\text{IV}} + n\text{H}_2\text{O} \rightarrow \text{An}^{\text{IV}}/(\text{H}_2\text{O})_n$ , cover the range of the MM BEs corresponding to the full extracted cluster set. The reference QM computations are performed at the MP2 level.

to the study of the  $\text{Th}^{\text{IV}}$  hydration [25]. That force field includes four main energy components : a repulsive, a Coulombic, a polarization (including short range damping effects) and a charge donation energy term (see Materials and Methods). Regarding water/water interactions, we consider the water polarizable model TCPE/2013 [30] mentioned in Introduction. Below, we denote "molecular modeling" (MM) the force-field results, and "QM" the quantum data.

Force-field parameters are assigned from the automated iterative procedure, summarized in Figure 1. All iterative procedure iterations consist in the sequence of: MD sampling, QM reference energy calculation (Binding Energies (BEs) corresponding to the reaction  $\text{An}^{\text{IV}} + n\text{H}_2\text{O} \rightarrow \text{An}^{\text{IV}}/(\text{H}_2\text{O})_n$  and different fragment interactions; see SI for definitions) and fitting process. The parameter initial guesses correspond to force-field parameters assigned from the GP-P procedure, *i.e.* the training data set corresponds to small hydrated  $\text{An}^{\text{IV}}$  clusters comprising at most 10 water molecules optimized in gas phase using high end QM methods. The training data set at each iterative procedure's iteration comprises all the clusters from the previous two iterations, ensuring the BP-P convergence stability to the final force field. As high end QM computations regarding  $\text{An}^{\text{IV}}$  are still par-

ticularly computationally expensive, the MD sampling consists in extracting 20 hydrated  $\text{An}^{\text{IV}}$  clusters (the cation plus its first hydration sphere); for each cluster, about 10 interaction energies are computed to obtain the BEs and different fragment interaction energies. To ensure that the 20 selected clusters at each iteration are representative, we checked that the MM BEs of these small clusters set span over the range of MM cluster BEs extracted from the full trajectory. At each iterative procedure's iteration, the evolution of the force-field parameters as well as structural properties (radial distribution function, and coordination number) is monitored, until the self-consistent solution is reached. Convergence is usually reached in less than 6 iterations. Examples are provided in the SI in section 4. Today all the computations of a single iterative procedure's iteration for the whole  $\text{An}^{\text{IV}}$  series can be performed at the week scale using a few percents of a modern supercomputing system (made of about 100,000 computing cores).

The improvement in the force-field quality arising from the iterative procedure may be assessed from the data plotted in Figure 2. In that figure, the classical BEs computed from the parameter initial guesses (GP-P) and from the BP-P converged force field are plotted a function of their QM reference counterparts for a training cluster set. If MM BEs from the initial parameter guesses are linearly correlated with QM ones, a large systematic deviation exists between the two BE sets, of about  $-22 \text{ kcal mol}^{-1}$ . If that represents only 2.5 % of the cluster BEs, that corresponds to about  $36 k_B T$  at ambient conditions. With the BP-P force field, the BE mean error is centered on 0 and its standard deviation is reduced to less than  $5 \text{ kcal mol}^{-1}$ . These results support the earlier conclusion Tazi et al. [36], *i.e.* force-field parameter adjustments relying on realistic bulk-phase structures ensures the accuracy of the resulting force-field.

## RESULTS AND DISCUSSION

The behavior of the whole  $\text{An}^{\text{IV}}$  series in 0.03 M cation aqueous solutions is studied by means of MD simulations at the 10 ns scale using the BP-P force fields. We don't account explicitly for counter ions in our bulk simulations. However as the simulations are performed using an Ewald summation scheme with tinfoil boundary conditions, the cations are accompanied by uniform canceling background charge, acting as an implicit dilute counter ion cloud. We also simulated accordingly the lanthanide  $\text{Ce}^{\text{IV}}$  that is inferred to present very close hydration properties as  $\text{Pu}^{\text{IV}}$ . From MD trajectories, relevant structural properties like the pair  $\text{An}^{\text{IV}}$ /water oxygen radial distribution functions, RDFs, the position  $d_{\text{AnO}}$  of the RDF first peak, and the cation hydration number  $N_c$  are estimated.

As expected from the  $\text{An}^{\text{IV}}$  large charge, MD simula-

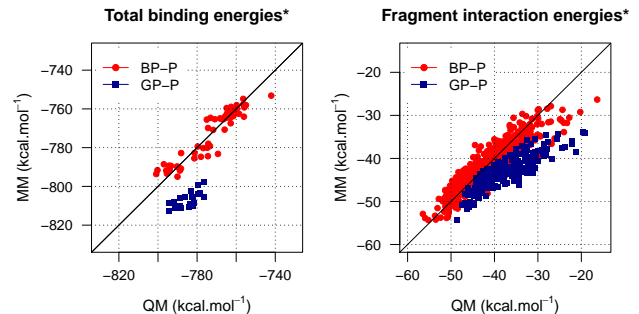


FIG. 2: Comparison of QM and MM binding energies BEs and of the fragment interaction energies, *i.e.* the interaction energy of a single water molecule of the  $\text{An}^{\text{IV}}(\text{H}_2\text{O})_n$  cluster with the remaining  $\text{An}^{\text{IV}}(\text{H}_2\text{O})_{n-1}$  fragment, for  $\text{Th}^{\text{IV}}$  when using the force-field parameter initial guess built from QM data corresponding to clusters optimized in gas phase (GP-P) and from the automated iterative procedure (BP-P). The mean error is reduced to less than  $0.1 \text{ kcal mol}^{-1}$  with a standard deviation of respectively 4.8 and  $2.6 \text{ kcal mol}^{-1}$  for the total BEs and the fragment interaction energies with the latter approach.

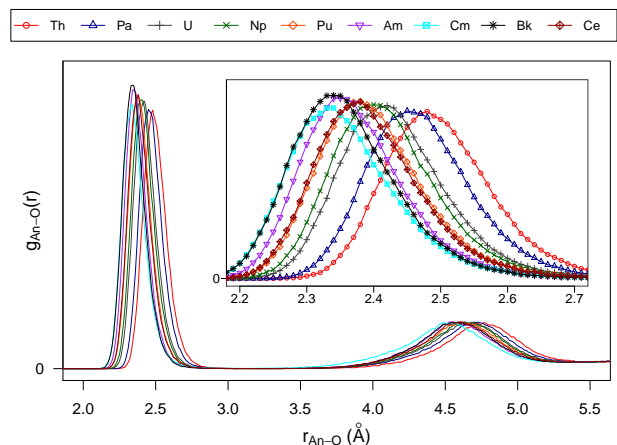


FIG. 3:  $\text{An}^{\text{IV}} - \text{O}$  pair radial distribution functions. **(Fonctions a normaliser!!!).**

tions show the cation surrounding water molecules to be organized in two well defined solvation shells (see Figure 3). At the exception of  $\text{Cm}^{\text{IV}}$ , the RDF first peak shifts in a very progressive fashion to shorter distances as the actinide gets heavier. The  $d_{\text{AnO}}$  distance decreases from  $\text{Th}^{\text{IV}}$  to  $\text{Cm}^{\text{IV}}$ , while the  $\text{Bk}^{\text{IV}}$  one is found to be slightly longer than for  $\text{Cm}^{\text{IV}}$ . Our  $d_{\text{AnO}}$  distance agree within at most  $0.02 \text{ Å}$  compared to available EXAFS data (see the Supporting Information Table S2). We plot on Figure 4 the  $d_{\text{AnO}}$  distances as a function of the  $\text{An}^{\text{IV}}$  ionic radii estimated from crystallographic data [18, 37].

The two series of data are linearly correlated. Following the idea of Warren and Patel [38], the ionic radii can be estimated from the distances  $d_{AnO}$  to which the water molecular radius is subtracted. For the TCPE/2013 model, the water radius is 1.393 Å [30]. That yields a nice agreement between the our computed radii and the crystallographic ones, within less than 0.02 Å (see Supporting Information).

The computed  $N_c$ 's start at 9.4 for Th and decrease until they reach a plateau of about 9 for the series Pa–Pu, Bk with Am and Cm moving down away from the series with a coordination number of respectively 8.7 and 8.3, see Figure 4. Compared to experimental data regarding solutions for which the counter ions are known to not enter the  $An^{IV}$  first hydration shell (i.e. mainly perchlorate anions),  $N_c$ 's for the  $\{Th^{IV} - Np^{IV}\}$  series are included within the experimental range, while the  $N_c$  values for  $Pu^{IV}$  and  $Bk^{IV}$  are one unit above the experimental values. However, the EXAFS uncertainty regarding  $N_c$  values being 10-20 %, our  $N_c$  values for  $Pu^{IV}$  and  $Bk^{IV}$  may be considered as agreeing with experiment, within the error bars.

The fractional  $N_c$ 's for  $Th^{IV}$ ,  $Pa^{IV}$ ,  $Am^{IV}$ ,  $Cm^{IV}$  and  $Bk^{IV}$ , reveal the existence of an equilibrium between two coordination modes. An analysis of the coordination polyhedra has been made with *ChemNetworks* [39] and shows that the 8 coordination mode is associated with the formation of either a square anti-prismatic or a biaugmented trigonal prismatic geometry of the water molecules around the actinide cation. The identified polyhedra for the 9 coordination number are either a tri-augmented trigonal prism or a mono-capped square anti-prism and for the 10 coordination number either a bi-capped square anti-prism or a sphenocorona. The corresponding structures for the observed polyhedra extracted from the MD trajectories can be found in Figure S3 of the SI.

We computed the mean residence time, MRT, of a water molecule within  $An^{IV}$  first hydration shell along the MD trajectories from the approach of Impey et al. [40]. The computed MRTs range from a few hundreds of picoseconds for  $Cm^{IV}$ ,  $Am^{IV}$  and  $Th^{IV}$  up to 1.5 ns for  $U^{IV}$ . Experimentally, only the  $U^{IV}$  MRT has been reported [41], about 185 ns, as well as an upper bound limit for  $Th^{IV}$ , 20 ns [41]. Our estimates are *a priori* from one to two orders of magnitude smaller than experiment. However we simulate here an 0.03 M  $An^{IV}$  aqueous solution, while these cations are studied experimentally in much more concentrated solutions. Moreover, the presence of explicit counter ions in the first and second cation hydration shells can also strongly affect the water dynamics at the cation vicinity. The quality of the present BP-P force field cannot be incriminated yet to explain the apparent disagreement between the computed and the rare experimental MRT estimates.

We computed the hydration free energies,  $\Delta G_{hyd}$ , for

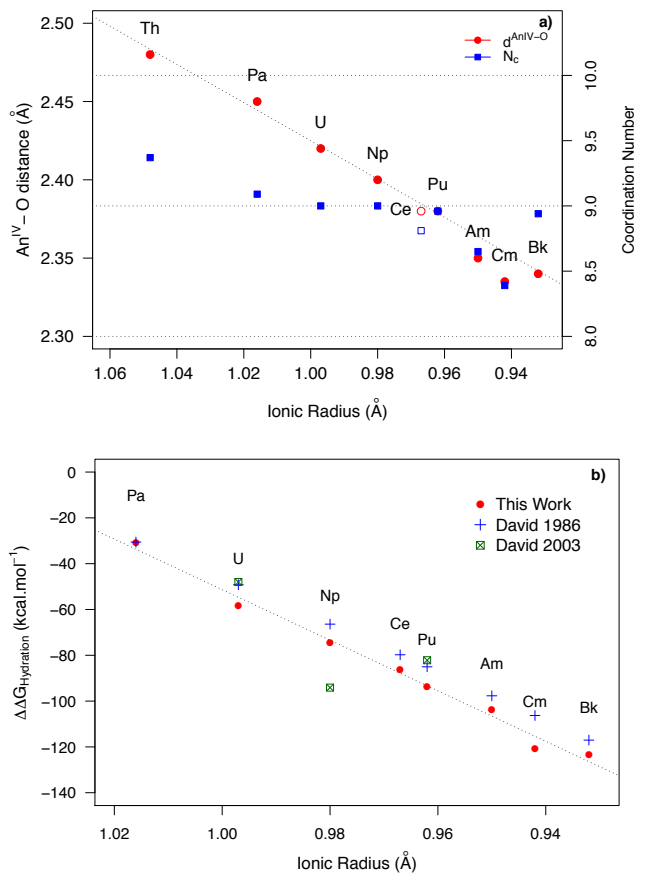


FIG. 4: (a) Distances  $d_{AnO}$  (red circles) as a function of ionic radii [18, 37]. The  $N_c$  estimates, computed by integrating the first RDF peak shown as blue squares in Figure 3, are reported on that plot (as the RDFs are null between their first and second peak the  $N_c$  error bar is zero). (b)  $An^{IV}$  hydration free energy relative to  $Th^{IV}$  ( $\Delta G_{hyd}$ ) versus the  $An^{IV}$  ionic radii. In dashed lines, the linear regression fit, the regression coefficients are 0.99 and 0.99 for (a) and (b) respectively.

the  $An^{IV}$  series relatively to  $Th^{IV}$  using the thermodynamic integration method. As for the distances  $d_{AnO}$ , we get again a linear correlation between our  $\Delta G_{hyd}$  values and the crystallographic ionic radii, as well as between our  $\Delta G_{hyd}$  values and the  $\Delta G_{hyd}$  ones computed from the David et al.'s model [18, 19] (in the latter case, at the exception of  $Np^{IV}$ , see our discussion in Introduction), see Figure 4. Our BP-P force fields predict the  $\Delta G_{hyd}$  values to smoothly decrease along the  $An^{IV}$  series. This is *a priori* in line with the continuous decrease of the  $d_{AnO}$  distances along that series that has to yield the reinforcement of  $An^{IV}$ /water interactions.

We also assigned BP-P parameters from the iterative procedure for the lanthanide element  $Ce^{IV}$ . We simulated then that element in an aqueous solution using the same computational protocol and simulation conditions

as above. From our simulations,  $\text{Ce}^{\text{IV}}$  exhibits a very similar behavior to  $\text{Pu}^{\text{IV}}$  in bulk water, with an identical  $d_{\text{AnO}}$  distance of 2.38 Å and close  $N_c$  values, of respectively 9.0 and 8.8, for  $\text{Pu}^{\text{IV}}$  and  $\text{Ce}^{\text{IV}}$ . The similarity is further consolidated while comparing the respective RDFs of both elements that can be almost superimposed. Lastly, concerning the  $\Delta G_{\text{hyd}}$  values, the  $\text{Ce}^{\text{IV}}$  estimate is found to be in between  $\text{Np}^{\text{IV}}$  and  $\text{Pu}^{\text{IV}}$ , still closer to the latter with a difference of 8 kcal mol<sup>-1</sup>. Such a level of similarities between hydrated  $\text{Ce}^{\text{IV}}$  and  $\text{Pu}^{\text{IV}}$  have been also reported from QM and experimental studies [42, 43].

Finally, considering the previous MD simulations reported in the literature, on the one hand, we find out that DFT-based MD generally underestimate the coordination number [21], while exhibiting the largest computed interaction distances (Table S2); while on the other hand, different classical MD for  $\text{Th}^{\text{IV}}$  give very large ranges of coordination numbers (from 8 to 11.4) and interaction distances (from 2.40 to 2.48 Å). This disparity further proves the need of highly accurate force-field parameters assignment protocol to reduce as far as possible all the drawbacks with mentioned in Introduction about building force fields.

## CONCLUSION

In this article we report the first polarizable  $\text{An}^{\text{IV}}-\text{H}_2\text{O}$  classical potentials derived from an automated iterative coherent *ab initio* methodology for the series from thorium to berkelium. We emphasize that the specific inclusion of sampled condensed phase reference structures in a self-consistent manner enables to reach an adequate accuracy necessary to simulate the actinide aqueous condensed phase systems. The hydration study from classical molecular dynamics with our newly developed force field reveals that, except for  $\text{Am}^{\text{IV}}$  and  $\text{Cm}^{\text{IV}}$  which sit aside the series, the structural and thermodynamical properties change in a very smooth fashion along the studied series. The first comparisons to experimental data exhibit a very good overall agreement. They will be extended in a near future by considering counter anions to achieve a thorougher comparability to experimental conditions. Nevertheless, these methodological developments pave the way for a better classical description of the +4 actinides in solution, and thus our ability to study their chemical behavior in more complex and chemically relevant systems; this being of special interest considering how important and challenging  $\text{Pu}^{\text{IV}}$  chemistry is with respect to the nuclear fuel cycle.

## MATERIAL METHODS

### QM calculations

All the QM calculations on the actinide aqua clusters have been performed with the Turbomole package [44], employing the unrestricted RI-MP2 method [45, 46] as mentioned in the introduction. For the actinides, the Stuttgart-Cologne "small core" relativistic effective core potential (60 e<sup>-</sup>) were used in conjunction with the associated segmented basis sets [47–49], while the augmented correlation consistent triple *zeta* basis sets of Dunning [50, 51], namely the aug-cc-pVTZ, were used for the water molecules. The actinides have all been considered in their high spin state for the calculations and the 1s core electrons of the oxygen as well as the 5s, 5p, 5d electrons of the actinides are not correlated in the MP2 step.

### Molecular Dynamics

The MD simulations of the  $\text{An}^{\text{IV}}$  in bulk water were conducted with a cubic box containing only one actinide cation for 1000 water molecules with periodic boundary conditions in PolarisMD package developed by one of us. The system is first equilibrated in volume and temperature in the {N,P,T} ensemble with a Noose-Hoover thermostat and barostat [52]. The different runs of production used for the parametrization and final analysis are then run in the canonical ensemble [53] during 5 ns always following a 1 ns re-equilibration. It should be recalled here that the water model used for the simulations is the latest TCPE version reported in ref [30]. The water molecule's structural parameters constrained to their bulk equilibrium values thanks to the RATTLE algorithm (the convergence criterium is set to 10<sup>-6</sup> Å). Since the constituents of the system have no free internal motion, the simulation time-step is fixed to 1 fs and, in order to minimize the extra computational expense inherent to the polarization model, the induced dipoles are accounted for within the multiple time step r-RESPAP framework [54]. The hydration free energies,  $\Delta G_{\text{hyd}}$  are computed relatively to  $\text{Th}^{\text{IV}}$  thanks to the thermodynamic integration methods. For each element, the  $\text{Th}^{\text{IV}}$  is alchemically transformed to the final element in 20 equally spaced steps in which the corresponding hamiltonian are mixed. For each step, we performed a 100 ps run of equilibration followed by a 500 ps one during which the thermostatical average is computed.

### Coordination mode analysis

We analyzed the coordination polyhedra using *Chem-Networks* [39]. The details of the analysis are reported

Figure S3.

## ACKNOWLEDGEMENTS

The members of the PhLAM laboratory acknowledge support from the CaPPA project (Chemical and Physical Properties of the Atmosphere) that is funded by the French National Research Agency (ANR) through the PIA (Programme d'Investissement d'Avenir) under contract "ANR-11-LABX-0005-0" and by the Regional Council "Hauts de France" and the "European Funds for Regional Economic Development" (FEDER) through the Contrat de Projets Etat-Région (CPER) CLIMIBIO (Changement climatique, dynamique de l'atmosphère, impacts sur la biodiversité et la santé humaine), and the OVERSEE project (MODélisation innoVante dEs aéRoSols dE radionucléidEs) supported by the I-SITE Université Lille Nord-Europe. Furthermore, this work was granted access to the HPC resources of [CINES/IDRIS/TGCC] under the allocation 2016-2018 [x2016081859 and A0010801859] made by GENCI.

---

\* Univ. Lille, CNRS, UMR 8523 – PhLAM – Physique des Lasers Atomes et Molécules, F-59000 Lille, France

- [1] K. L. Nash, C. Madic, and J. N. Mathur, in *The Chemistry of the Actinide and Transactinide Elements*, Vol. 4, Chap. 24, pp. 2622–2798.
- [2] K. E. Knope and L. Soderholm, *Chem. Rev.* **113**, 944 (2013).
- [3] H. Moll, M. A. Denecke, F. Jalilehvand, M. Sandström, and I. Grenthe, *Inorg. Chem.* **38**, 1795 (1999).
- [4] N. Torapava, I. Persson, L. Eriksson, and D. Lundberg, *Inorg. Chem.* **48**, 11712 (2009).
- [5] C. Hennig, K. Schmeide, V. Brendler, H. Moll, S. Tsushima, and A. C. Scheinost, *Inorg. Chem.* **46**, 5882 (2007).
- [6] V. Neck, R. Muller, M. Bouby, M. Altmaier, J. Rothe, M. A. Denecke, and J. I. Kim, *Radiochim. Acta* **90**, 485 (2002).
- [7] R. E. Wilson, S. Skanthakumar, P. C. Burns, and L. Soderholm, *Angew. Chem. Int. Ed.* **46**, 8043 (2007).
- [8] N. L. Banik, V. Vallet, F. Réal, R. M. Belméchéri, B. Schimmelpfennig, J. Rothe, R. Marsac, P. Lindqvist-Reis, C. Walther, M. A. Denecke, and C. M. Marquardt, *Dalton Trans.* **45**, 453 (2016).
- [9] A. Ikeda-Ohno, C. Hennig, S. Tsushima, A. C. Scheinost, G. Bernhard, and T. Yaita, *Inorg. Chem.* **48**, 7201 (2009).
- [10] C. Hennig, J. Tutschku, A. Rossberg, G. Bernhard, and A. C. Scheinost, *Inorg. Chem.* **44**, 6655 (2005).
- [11] M. R. Antonio, L. Soderholm, C. W. Williams, J.-P. Blaudeau, and B. E. Bursten, *Radiochim. Acta* **89**, 17 (2001).
- [12] A. Ikeda-Ohno, C. Hennig, A. Rossberg, H. Funke, A. C. Scheinost, G. Bernhard, and T. Yaita, *Inorg. Chem.* **47**, 8294 (2008).
- [13] M. A. Denecke, K. Dardenne, and C. M. Marquardt, *Talanta* **65**, 1008 (2005).
- [14] J. Rothe, C. Walther, M. A. Denecke, and T. Fanghänel, *Inorg. Chem.* **43**, 4708 (2004).
- [15] K. Dardenne, A. Seibert, M. A. Denecke, and C. M. Marquardt, *Radiochim. Acta* **97**, 91 (2009).
- [16] M. R. Antonio, C. W. Williams, and L. Soderholm, *Radiochim. Acta* **90**, 851 (2002).
- [17] T. K. Sham, *Phys. Rev. B* **40**, 6045 (1989).
- [18] F. David, *J. Less-Common Met.* **121**, 27 (1986), proceedings of Actinides 85, Aix en Provence - Part I.
- [19] F. H. David and V. Vokhmin, *New J. Chem.* **27**, 1627 (2003).
- [20] R. Spezia, C. Beuchat, R. Vuilleumier, P. D'Angelo, and L. Gagliardi, *J. Phys. Chem. B* **116**, 6465 (2012).
- [21] R. Atta-Fynn, D. F. Johnson, E. J. Bylaska, E. S. Ilton, G. K. Schenter, and W. A. de Jong, *Inorg. Chem.* **51**, 3016 (2012).
- [22] S. O. Odoh, E. J. Bylaska, and W. A. de Jong, *J. Phys. Chem. A* **117**, 12256 (2013).
- [23] R. Spezia, Y. Jeanvoine, C. Beuchat, L. Gagliardi, and R. Vuilleumier, *Phys. Chem. Chem. Phys.* **16**, 5824 (2014).
- [24] R. Atta-Fynn, E. J. Bylaska, and W. A. de Jong, *J. Phys. Chem. A* **120**, 10216 (2016).
- [25] F. Réal, M. Trumm, V. Vallet, B. Schimmelpfennig, M. Masella, and J.-P. Flament, *J. Phys. Chem. B* **114**, 15913 (2010).
- [26] A. Zen, Y. Luo, G. Mazzola, L. Guidoni, and S. Sorella, *J. Chem. Phys.* **142**, 144111 (2015).
- [27] J. Liu, X. He, J. Z. H. Zhang, and L.-W. Qi, *Chem. Sci.* **9**, 2065 (2018).
- [28] L. Hemmingsen, P. Amara, E. Ansorbóro, and M. J. Field, *J. Phys. Chem. A* **104**, 4095 (2000).
- [29] C. Clavaguéra-Sarrio, V. Brenner, S. Hoyau, C. J. Marsden, P. Millié, and J.-P. Dognon, *J. Phys. Chem. B* **107**, 3051 (2003).
- [30] F. Réal, V. Vallet, J.-P. Flament, and M. Masella, *J. Chem. Phys.* **139**, 114502 (2013).
- [31] A. Marjolin, C. Gourlaouen, C. Clavaguéra, P. Ren, J. Wu, N. Gresh, J.-P. Dognon, and J.-P. Piquemal, *Theor. Chem. Acc.* **131**, 1 (2012).
- [32] F. Réal, M. Trumm, B. Schimmelpfennig, M. Masella, and V. Vallet, *J. Comput. Chem.* **34**, 707 (2013).
- [33] E. Galbis, J. Hernández-Cobos, R. R. Pappalardo, and E. S. Marcos, *J. Chem. Phys.* **140**, 214104 (2014).
- [34] F. Fracchia, G. Del Frate, G. Mancini, W. Rocchia, and V. Barone, *J. Chem. Theory Comput.* **14**, 255 (2017).
- [35] D. G. Kolman, Y. Park, M. Stan, R. J. Hanrahan Jr, and D. P. Butt, *Report LA-UR-99-0419*, Tech. Rep. (1999).
- [36] S. Tazi, J. J. Molina, B. Rotenberg, P. Turq, R. Vuilleumier, and M. Salanne, *J. Chem. Phys.* **136**, 114507 (2012).
- [37] R. D. Shannon, *Acta Crystallogr. A* **32**, 751 (1976).
- [38] G. L. Warren and S. Patel, *J. Chem. Phys.* **127**, 064509 (2007).
- [39] A. Ozkanlar and A. E. Clark, *J. Comput. Chem.* **35**, 495 (2014).
- [40] R. W. Impey, P. A. Madden, and I. R. McDonald, *J. Phys. Chem.* **87**, 5071 (1983).
- [41] I. Farkas, I. Grenthe, and I. Bányai, *J. Phys. Chem. A* **104**, 1201 (2000).
- [42] M. Šulka, L. Cantrel, and V. Vallet, *J. Phys. Chem. A* **118**, 10073 (2014).

- [43] R. Marsac, F. Real, N. L. Banik, M. Pedrot, O. Pourret, and V. Vallet, *Dalton Trans.* **46**, 13553 (2017).
- [44] “TURBOMOLE V7.1 2016, a development of University of Karlsruhe and Forschungszentrum Karlsruhe GmbH, 1989-2007, TURBOMOLE GmbH, since 2007; available from <http://www.turbomole.com>”.
- [45] C. Hättig, A. Hellweg, and A. Köhn, *Phys. Chem. Chem. Phys.* **8**, 1159 (2006).
- [46] C. Hättig and F. Weigend, *J. Chem. Phys.* **113**, 5154 (2000).
- [47] X. Cao and M. Dolg, *J. Mol. Struct. (Theochem)* **673**, 203 (2004).
- [48] X. Cao, M. Dolg, and H. Stoll, *J. Chem. Phys.* **118**, 487 (2003).
- [49] W. Küchle, M. Dolg, H. Stoll, and H. Preuss, *J. Chem. Phys.* **100**, 7535 (1994).
- [50] T. H. Dunning, Jr., *J. Chem. Phys.* **90**, 1007 (1989).
- [51] C. Hättig, *Phys. Chem. Chem. Phys.* **7**, 59 (2005).
- [52] G. J. Martyna, M. E. Tuckerman, D. J. Tobias, and M. L. Klein, *Mol. Phys.* **87**, 1117 (1996).
- [53] Y. Liu and M. E. Tuckerman, *J. Chem. Phys.* **112**, 1685 (2000).
- [54] M. Masella, *Mol. Phys.* **104**, 415 (2006).

Supporting information for:

Properties of the tetravalent actinide series in  
aqueous phase a microscopic simulation  
automated engine

Eléonor Acher,<sup>†</sup> Michel Masella,<sup>¶</sup> Valérie Vallet,<sup>§</sup> and Florent Réal<sup>\*,§</sup>

<sup>†</sup>*CEA, Nuclear Energy Division, Research Department on Mining and fuel Recycling  
Processes (LILA), BP17171 F-30207 Bagnols-sur-Cèze, France*

<sup>‡</sup>*Univ. Lille, CNRS, UMR 8523 – PhLAM – Physique des Lasers Atomes et Molécules,  
F-59000 Lille, France*

<sup>¶</sup>*Laboratoire de Biologie Structurale et Radiobiologie, Service de Bioénergétique, Biologie  
Structurale et Mécanismes, Institut Joliot, CEA Saclay, F-91191 Gif sur Yvette Cedex,  
France*

<sup>§</sup>*Université de Lille, CNRS, UMR 8523 – PhLAM – Physique des Lasers, Atomes et  
Molécules, F-59000 Lille*

E-mail: [florent.real@univ-lille.fr](mailto:florent.real@univ-lille.fr)

## List of Tables

S1	Force-field parameters for the series of $\text{An}^{\text{IV}}-\text{H}_2\text{O}$ potentials . . . . .	S10
S2	Comparison of structural MD computed data for the series of $\text{An}^{\text{IV}}-\text{water}$ with <i>GP-P</i> and <i>BP-P</i> to experimental EXAFS data and other MD simulations.	S10
S3	Mean Residence Time ( $\tau$ ) in nanosecond of a water molecule in the first co- ordination sphere of the $\text{An}^{\text{IV}}$ . . . . .	S11
S4	Hydration free energies of the $\text{Th}^{\text{IV}}-\text{Bk}^{\text{IV}}$ tetravalent actinide series and $\text{Ce}^{\text{IV}}$ relative to thorium ( $\text{kcal mol}^{-1}$ ), and ionic radii in Å . . . . .	S11

## List of Figures

S1	Differences between DFT and MP2 calculated on twenty clusters extracted from $\text{Th}^{\text{IV}}$ MD for (left) total binding energy and (right) fragment interaction energies. For the total binding energies, the double peaks correspond to different coordination numbers ( $\text{Th}^{\text{IV}}(\text{H}_2\text{O})_{10}$ and $\text{Th}^{\text{IV}}(\text{H}_2\text{O})_9$ here). . . . .	<a href="#">S5</a>
S2	Convergence of (a) FF parameters, (c) coordination number and $\text{An}^{\text{IV}}-\text{H}_2\text{O}$ interaction distances for $\text{Th}^{\text{IV}}$ , $\text{Pu}^{\text{IV}}$ and $\text{Bk}^{\text{IV}}$ . (b) Evolution of the $\text{Th}^{\text{IV}}-\text{O}$ radial distribution function (RDF) along the iterations of the sampling of the solvated phase procedure <i>BP-P</i> . . . . .	<a href="#">S9</a>
S3	Observed polyhedra for the coordination numbers (CN) ranging from 8 to 10	<a href="#">S11</a>

# 1 Comments on the accuracy of DFT for total binding energies and fragment interaction energies

In the present study, we chose to compute all cluster binding energies and fragment interaction energies at the correlated MP2 level of theory, but one may question the accuracy of available functionals of the density (DFT), which depends on the simultaneous accuracies of actinide-water and water-water interactions. Réal *et al*<sup>S1</sup> showed that GGA (BP86), a hybrid (B3LYP), and meta-GGA (M06) functionals all overestimate the Th(IV)-water interaction energy by up to 18 kcal mol<sup>-1</sup>. Furthermore, most functionals exhibit excessive repulsions.<sup>S2</sup> In Figure S1, we have compared the total binding energies and fragment interaction energies (interaction energy between a water molecule and the An<sup>IV</sup>(H<sub>2</sub>O)<sub>*n*-1</sub> cluster, computed with two GGA functionals, BLYP, PBE, one hybrid functional, PBE0, and the dispersion corrected BLYP+D3 one. All four functionals of the density overestimate the fragment interaction energies, confirming the fact that water-water repulsions are overestimated. This error is not counterbalanced by the bias in the metal-water interactions; while BLYP overestimates total binding energies, PBE, PBE0, and BLYP+D3 yield to negative deviations, the larger the hydration number the larger the deviation from MP2 energies. This confirms that currently available functionals are not accurate enough to be used for the calculations of the QM reference energies.

## 2 Modeling ion/water interactions

As in our previous study,<sup>S1</sup> the force field used to model ion/water interactions is based on the following decomposition of the total potential energy

$$U = U_{\text{qq}'} + U_{\text{rep}} + U_{\text{ct}} + U_{\text{pol}}. \tag{1}$$

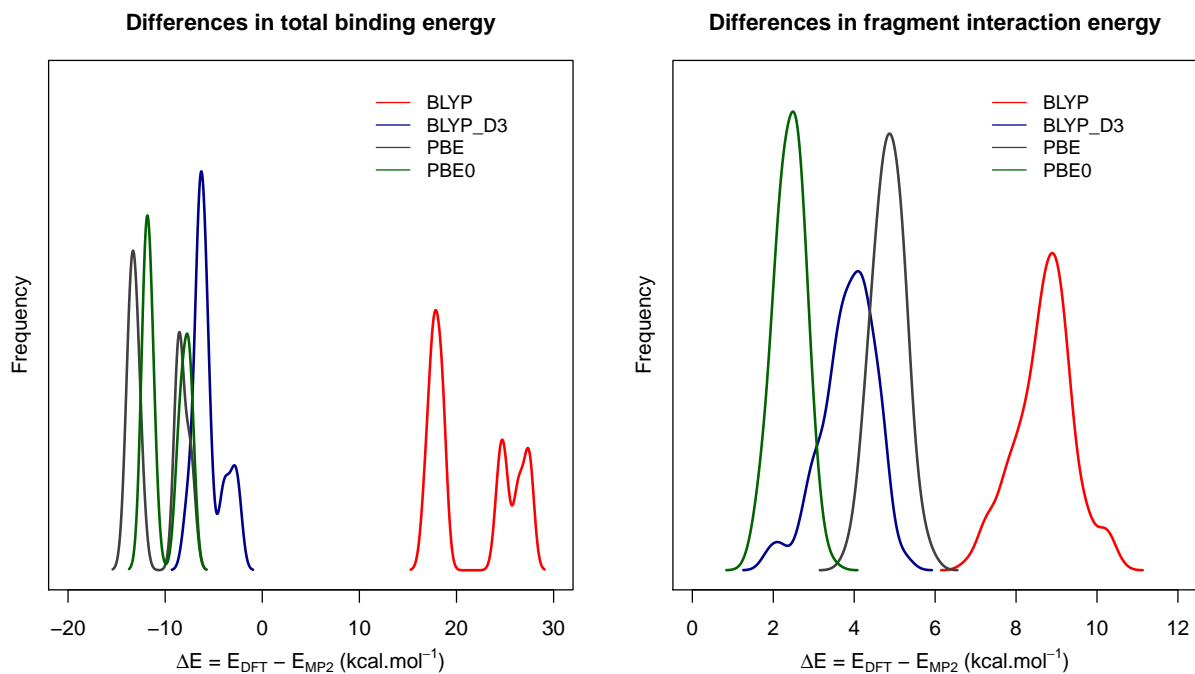


Figure S1: Differences between DFT and MP2 calculated on twenty clusters extracted from Th<sup>IV</sup> MD for (left) total binding energy and (right) fragment interaction energies. For the total binding energies, the double peaks correspond to different coordination numbers (Th<sup>IV</sup>(H<sub>2</sub>O)<sub>10</sub> and Th<sup>IV</sup>(H<sub>2</sub>O)<sub>9</sub> here).

The different terms correspond respectively to a classical charge-charge electrostatic, a repulsive, a specific charge-transfer and a polarization term. Conversely to our previous work, where the charge transfer term was taken as non-additive, here, the first three terms are additive potentials. On the contrary, the polarization term  $U_{pol}$  is based on a many-body induced dipole moment approach.

The repulsion is taken as decreasing exponential according to

$$U_{rep} = \sum_i A_{An-i} \exp(-b_{An-i} r_{An-i}). \quad (2)$$

For the charge-transfer term  $U_{ct}$ , which is introduced to account for the partial "covalent" character of the actinide/water interactions, we consider a classical exponential energy contribution:

$$U_{ct} = \sum_i D_{An-i}^{ct} \exp\left(-\frac{r_{An-i}}{\beta_{An-i}}\right). \quad (3)$$

The polarization energy term includes both anion/water and water/water interactions and  $U^{pol}$  is defined as:

$$U_{pol} = \frac{1}{2} \sum_{i=1}^{N_\mu} \frac{\mathbf{p}_i^2}{\alpha_i} - \sum_{i=1}^{N_\mu} \mathbf{p}_i \cdot \mathbf{E}_i^q - \frac{1}{2} \sum_{i=1}^{N_\mu} \sum_{j=1}^{N_\mu^*} \mathbf{p}_i \mathbf{T}_{ij} \mathbf{p}_j. \quad (4)$$

Here, the superscript \* indicates that the corresponding sum includes only pairs of atoms separated by more than two chemical bonds. Only non-hydrogen atoms are considered as polarizable centers, with an isotropic polarizability  $\alpha_i$  and an induced dipole moment  $\mathbf{p}_i$  expressed as

$$\mathbf{p}_i = \alpha_i \cdot \left( \mathbf{E}_i^q + \sum_{j=1}^{N_\mu^*} \mathbf{T}_{ij} \cdot \mathbf{p}_j \right). \quad (5)$$

$\mathbf{T}_{ij}$  is the dipolar interaction tensor and  $\mathbf{E}_i^q$  is the electric field generated on the polarizable center  $i$  by the surrounding static charges  $q_j$ . However,  $\mathbf{T}_{ij}$  and  $\mathbf{E}_i^q$  both include in our polarization approach an intermolecular short-range damping effect, according to the model

proposed by Thole<sup>S3</sup> according to

$$\rho(r) = \frac{3\kappa}{4\pi} \times \exp(-\kappa r^3), \quad (6)$$

where  $r$  is the distance from the atomic center and  $\kappa$ , s-called damping term, an adjustable parameter.

### 3 QM reference data

For both *GP-P* and *BP-P*, the reference total binding energy is calculated according to the chemical reaction  $\text{An}^{\text{IV}} + n \text{H}_2\text{O} \longrightarrow \text{An}^{\text{IV}}(\text{H}_2\text{O})_n$  and thus with the equation  $BE = E_{\text{An}^{\text{IV}}(\text{H}_2\text{O})_n} - E_{\text{An}^{\text{IV}}} - nE_{\text{H}_2\text{O}}$ . This energy is then corrected from the basis set superposition error between the actinides and the water molecules following the well established counterpoise correction method with the equation:

$$BSSE = E_{\text{An}^{\text{IV}}(\text{H}_2\text{O})_n}^{\text{An}^{\text{IV}}} - E_{\text{An}^{\text{IV}}}^{\text{An}^{\text{IV}}} + E_{(\text{H}_2\text{O})_n}^{\text{An}^{\text{IV}}(\text{H}_2\text{O})_n} - E_{(\text{H}_2\text{O})_n}^{(\text{H}_2\text{O})_n}, \quad (7)$$

where the subscript refers to the fragment considered and the superscript to the used basis set. The corrected total binding energy is then:

$$BE^{cpc} = E_{\text{An}^{\text{IV}}(\text{H}_2\text{O})_n} - E_{\text{An}^{\text{IV}}}^{\text{An}^{\text{IV}}(\text{H}_2\text{O})_n} - E_{(\text{H}_2\text{O})_n}^{\text{An}^{\text{IV}}(\text{H}_2\text{O})_n} + E_{(\text{H}_2\text{O})_n} - nE_{\text{H}_2\text{O}}, \quad (8)$$

where the superscript has been omitted when the basis set used is the fragment's own basis set.

The second reference data that we call fragment interaction energy is the counterpoise corrected interaction energy defined according to the equation:

$$E_{int}^{cpc} = E_{AB}^{AB} - E_A^{AB} - E_B^{AB}, \quad (9)$$

with the fragments  $A$  and  $B$  corresponding to, on the one hand to a single water molecule of the  $\text{An}^{\text{IV}}(\text{H}_2\text{O})_n$  cluster and on the other hand to the remaining atoms.

## 4 *BP-P* convergence

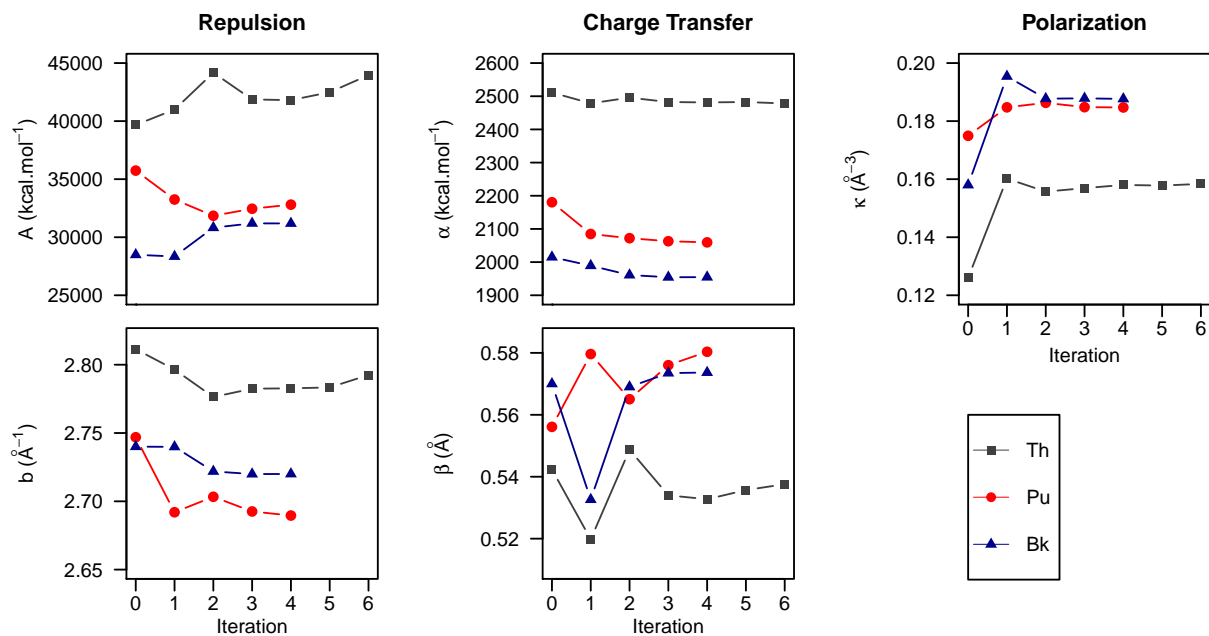
Figure S2 (a) illustrates that the five FF parameters for Th, Pu, and Bk converge after 3-5 iterations, as the training data sets is updated with sampled snapshots from classical MD simulations. The convergence of the An–H<sub>2</sub>O interaction distances and radial distribution functions as well as average coordination numbers can also be visualized on Figure S2 subsets (b) and (c).

## 5 Final parameters

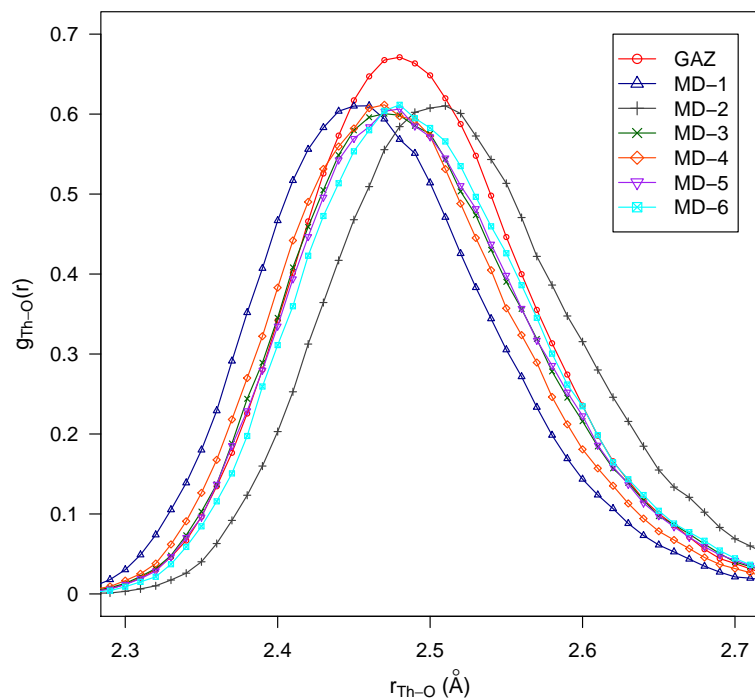
The actinide charges for coulombic and polarization are fixed to their +4 net charge and their polarizability is either fixed to the QM values reported in the literature<sup>S4,S5</sup> or fixed to 1 Å<sup>3</sup>, the latter assumption not exhibiting any significant impact on the interaction energies. Considering that the water potential parameters are fixed, only five parameters need to be adjusted with the Model-Independent Parameter Estimation (PEST) software package;<sup>S6</sup> namely the repulsion  $A_{\text{An}-i}$  and  $b_{\text{An}-i}$ , the charge transfer  $D_{\text{An}-i}$  and  $\beta_{\text{An}-i}$  and the Thole damping one  $\kappa$ .

## References

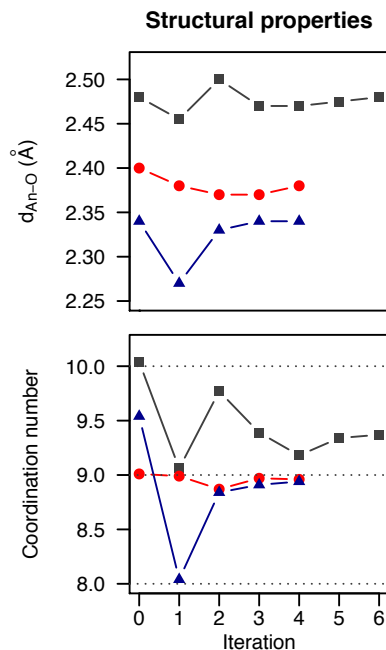
- (S1) Réal, F.; Trumm, M.; Vallet, V.; Schimmelpfennig, B.; Masella, M.; Flament, J.-P. Quantum Chemical and Molecular Dynamics Study of the Coordination of Th(IV) in Aqueous Solvent. *J. Phys. Chem. B* **2010**, *114*, 15913–15924, DOI: 10.1021/jp108061s.



(a) Force-field parameters.



(b) Th<sup>IV</sup>-O RDF.



(c) Structural properties.

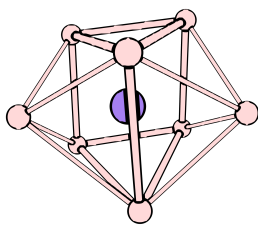
Figure S2: Convergence of (a) FF parameters, (c) coordination number and An<sup>IV</sup>-H<sub>2</sub>O interaction distances for Th<sup>IV</sup>, Pu<sup>IV</sup> and Bk<sup>IV</sup>. (b) Evolution of the Th<sup>IV</sup>-O radial distribution function (RDF) along the iterations of the sampling of the solvated phase procedure *BP-P*.

Table S1: Force-field parameters for the series of  $\text{An}^{\text{IV}}-\text{H}_2\text{O}$  potentials

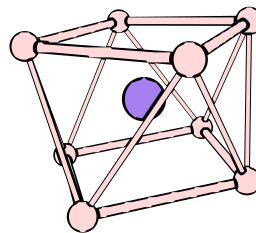
	Element	$A$ (kcal mol <sup>-1</sup> )	$b$ ( <sup>-1</sup> )	$D^{ct}$ (kcal mol <sup>-1</sup> )	$\beta$ (Å)	$\kappa$ ( <sup>-3</sup> )	$\alpha$ ( <sup>3</sup> )
$GP-P$	Th	39673	2.81	2511	0.54	0.126	1.142
	Pa	33783	2.75	2197	0.56	0.140	1.217
	U	30391	2.72	2034	0.57	0.148	1.180
	Np	26456	2.68	1715	0.59	0.146	1.063
	Pu	30692	2.76	2027	0.57	0.148	1.063
	Am	20823	2.57	1060	0.67	0.178	1.000
	Cm	19251	2.55	770	0.73	0.180	1.000
	Bk	28490	2.74	2015	0.57	0.158	1.000
	Ce	22081	2.60	1074	0.66	0.164	0.860
$BP-P$	Th	43960	2.792	2478	0.538	0.158	1.142
	Pa	42997	2.756	2396	0.559	0.176	1.217
	U	36135	2.704	2395	0.561	0.179	1.180
	Np	36402	2.725	2208	0.568	0.182	1.116
	Pu	32808	2.690	2060	0.580	0.185	1.063
	Am	50976	2.930	2108	0.543	0.208	1.000
	Cm	35532	2.707	2015	0.590	0.215	1.000
	Bk	31187	2.720	1955	0.574	0.188	1.000
	Ce	42891	2.867	1348	0.591	0.197	0.860

 Table S2: Comparison of structural MD computed data for the series of  $\text{An}^{\text{IV}}-\text{water}$  with *GP-P* and *BP-P* to experimental EXAFS data and other MD simulations.

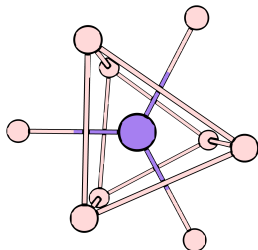
Elt	<i>GP-P</i>		<i>BP-P</i>		Other MD simulations			Experiment		
	CN	$d_{\text{An-O}}$ (Å)	CN	$d_{\text{An-O}}$ (Å)	CN	$d_{\text{An-O}}$ (Å)	refs	CN	$d_{\text{An-O}}$ (Å)	ref
Th	10.0	2.48	9.4	2.48	8 - 11.4	2.40 - 2.50	<a href="#">S1,S7-S10</a>	9.0 - 12.7	2.44 - 2.46	<a href="#">S11-S15</a>
Pa	10.0	2.44	9.1	2.45	-	-	-	-	2.43	<a href="#">S16</a>
U	9.9	2.41	9.0	2.42	8.7 - 9	2.45	<a href="#">S17,S18</a>	8.7 - 10.6	2.40 - 2.42	<a href="#">S11,S19</a>
Np	9.9	2.40	9.0	2.40	-	-	-	8.7 - 10.4	2.37 - 2.40	<a href="#">S21-S23</a>
Pu	10.0	2.39	9.0	2.38	8.1	2.41	<a href="#">S24</a>	7.8 - 8.4	2.38 - 2.39	<a href="#">S25,S26</a>
Am	9.0	2.33	8.7	2.35	-	-	-	-	-	-
Cm	8.9	2.32	8.3	2.335	-	-	-	-	-	-
Bk	9.5	2.34	8.9	2.34	-	-	-	7.9	2.32	<a href="#">S27</a>
Ce	9.1	2.365	8.8	2.38	9	2.44	<a href="#">S28</a>	< 9	2.42	<a href="#">S29</a>



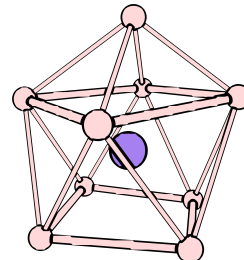
(a) Biaugmented Trigonal Prism (CN=8)



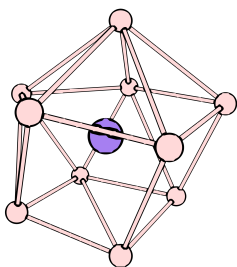
(b) Square Antiprism (CN=8)



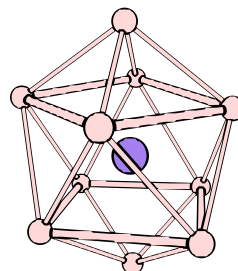
(c) Triaugmented Trigonal Prism (CN=9)



(d) Monocapped Square Antiprism (CN=9)



(e) Sphenocorona (CN=10)



(f) Bicapped Square Antiprism (CN=10)

Figure S3: Observed polyhedra for the coordination numbers (CN) ranging from 8 to 10

Table S3: Mean Residence Time ( $\tau$ ) in nanosecond of a water molecule in the first coordination sphere of the  $An^{IV}$ .

$\tau$ (ns)	Th	Pa	U	Np	Pu	Am	Cm	Bk	Ce
MD	0.6	0.9	1.5	1.4	1.1	0.5	0.3	1.0	0.5
Exp <sup>S30</sup>	< 20		$\approx 185$						

Table S4: Hydration free energies of the  $Th^{IV}$ - $Bk^{IV}$  tetravalent actinide series and  $Ce^{IV}$  relative to thorium ( $kcal\ mol^{-1}$ ), and ionic radii in Å

Element	Pa	U	Np	Pu	Am	Cm	Bk	Ce	Th (absolute)
This work	-31	-58	-74	-94	-104	-121	-123	-86	
David 1986 <sup>S31</sup>	-31	-49	-66	-85	-98	-106	-117	-80	-1446
David 2003 <sup>S32</sup>		-48	-94	-82					-1457
ionic radii <sup>S31,S33</sup>	1.016	0.997	0.980	0.962	0.950	0.942	0.932	0.967	1.048

- (S2) Gillan, M. J.; Alfè, D.; Michaelides, A. Perspective: How good is DFT for water? *J. Chem. Phys.* **2016**, *144*, 130901, DOI: 10.1063/1.4944633.
- (S3) Thole, B. Molecular polarizabilities calculated with a modified dipole interaction. *Chem. Phys.* **1981**, *59*, 341 – 350, DOI: 10.1016/0301-0104(81)85176-2.
- (S4) Parmar, P.; Peterson, K. A.; Clark, A. E. Static Electric Dipole Polarizabilities of Tri- and Tetravalent U, Np, and Pu Ions. *J. Phys. Chem. A* **2013**, *117*, 11874–11880, DOI: 10.1021/jp403078j.
- (S5) Réal, F.; Vallet, V.; Clavaguéra, C.; Dognon, J.-P. In silico prediction of atomic static electric dipole polarizabilities of the early tetravalent actinide ions:  $\text{Th}^{4+}$  ( $5f^0$ ),  $\text{Pa}^{4+}$  ( $5f^1$ ), and  $\text{U}^{4+}$  ( $5f^2$ ). *Phys. Rev. A* **2008**, *78*, 052502, DOI: 10.1103/PhysRevA.78.052502.
- (S6) Doherty, J. PEST: Model-Independent Parameter Estimation and Uncertainty Analysis. 2016; see <http://www.pesthomepage.org>.
- (S7) Atta-Fynn, R.; Bylaska, E. J.; de Jong, W. A. Strengthening of the Coordination Shell by Counter Ions in Aqueous  $\text{Th}^{4+}$  Solutions. *J. Phys. Chem. A* **2016**, *120*, 10216–10222, DOI: 10.1021/acs.jpca.6b09878.
- (S8) Marjolin, A.; Gurlaouen, C.; Clavaguéra, C.; Ren, P.; Wu, J.; Gresh, N.; Dognon, J.-P.; Piquemal, J.-P. Toward accurate solvation dynamics of lanthanides and actinides in water using polarizable force fields: from gas-phase energetics to hydration free energies. *Theor. Chem. Acc.* **2012**, *131*, 1–14, DOI: 10.1007/s00214-012-1198-7.
- (S9) Réal, F.; Trumm, M.; Schimmelpfennig, B.; Masella, M.; Vallet, V. Further insights in the ability of classical nonadditive potentials to model actinide ion–water interactions. *J. Comput. Chem.* **2013**, *34*, 707–719, DOI: 10.1002/jcc.23184.

- (S10) Spezia, R.; Beuchat, C.; Vuilleumier, R.; D’Angelo, P.; Gagliardi, L. Unravelling the Hydration Structure of  $\text{ThX}_4$  ( $\text{X} = \text{Br}, \text{Cl}$ ) Water Solutions by Molecular Dynamics Simulations and X-ray Absorption Spectroscopy. *J. Phys. Chem. B* **2012**, *116*, 6465–6475, DOI: 10.1021/jp210350b.
- (S11) Moll, H.; Denecke, M. A.; Jalilehvand, F.; Sandström, M.; Grenthe, I. Structure of the aqua ions and fluoride complexes of uranium(IV) and thorium(IV) in aqueous solution an EXAFS study. *Inorg. Chem.* **1999**, *38*, 1795–1799, DOI: 10.1021/ic981362z.
- (S12) Torapava, N.; Persson, I.; Eriksson, L.; Lundberg, D. Hydration and Hydrolysis of Thorium(IV) in Aqueous Solution and the Structures of Two Crystalline Thorium(IV) Hydrates. *Inorg. Chem.* **2009**, *48*, 11712–11723, DOI: 10.1021/ic901763s.
- (S13) Hennig, C.; Schmeide, K.; Brendler, V.; Moll, H.; Tsushima, S.; Scheinost, A. C. EXAFS Investigation of U(VI), U(IV), and Th(IV) Sulfato Complexes in Aqueous Solution. *Inorg. Chem.* **2007**, *46*, 5882–5892, DOI: 10.1021/ic0619759.
- (S14) Neck, V.; Muller, R.; Bouby, M.; Altmaier, M.; Rothe, J.; Denecke, M. A.; Kim, J. I. Solubility of amorphous Th(IV) hydroxide – application of LIBD to determine the solubility product and EXAFS for aqueous speciation. *Radiochim. Acta* **2002**, *90*, 485–494.
- (S15) Wilson, R. E.; Skanthakumar, S.; Burns, P. C.; Soderholm, L. Structure of the homoleptic thorium(IV) aqua ion  $[\text{Th}(\text{H}_2\text{O})_{10}]\text{Br}_4$ . *Angew. Chem. Int. Ed.* **2007**, *46*, 8043–8045, DOI: 10.1002/anie.200702872.
- (S16) Banik, N. L.; Vallet, V.; Réal, F.; Belméchéri, R. M.; Schimmelpfennig, B.; Rothe, J.; Marsac, R.; Lindqvist-Reis, P.; Walther, C.; Denecke, M. A.; Marquardt, C. M. First structural characterization of Pa(IV) in aqueous solution and quantum chemical investigations of the tetravalent actinides up to Bk(IV): the evidence of a curium break. *Dalton Trans.* **2016**, *45*, 453–457, DOI: 10.1039/c5dt03560k.

- (S17) Atta-Fynn, R.; Johnson, D. F.; Bylaska, E. J.; Ilton, E. S.; Schenter, G. K.; de Jong, W. A. Structure and Hydrolysis of the U(IV), U(V), and U(VI) Aqua Ions from Ab Initio Molecular Simulations. *Inorg. Chem.* **2012**, *51*, 3016–3024, DOI: 10.1021/ic202338z.
- (S18) Frick, R. J.; Pribil, A. B.; Hofer, T. S.; Randolph, B. R.; Bhattacharjee, A.; Rode, B. M. Structure and Dynamics of the  $\text{U}^{4+}$  Ion in Aqueous Solution: An ab Initio Quantum Mechanical Charge Field Molecular Dynamics Study. *Inorg. Chem.* **2009**, *48*, 3993–4002, DOI: 10.1021/ic801554p.
- (S19) Ikeda-Ohno, A.; Hennig, C.; Tsushima, S.; Scheinost, A. C.; Bernhard, G.; Yaita, T. Speciation and Structural Study of U(IV) and -(VI) in Perchloric and Nitric Acid Solutions. *Inorg. Chem.* **2009**, *48*, 7201–7210, DOI: 10.1021/ic9004467.
- (S20) Hennig, C.; Tutschku, J.; Rossberg, A.; Bernhard, G.; Scheinost, A. C. Comparative EXAFS Investigation of Uranium(VI) and -(IV) Aquo Chloro Complexes in Solution Using a Newly Developed Spectroelectrochemical Cell. *Inorg. Chem.* **2005**, *44*, 6655–6661, DOI: 10.1021/ic048422n.
- (S21) Antonio, M. R.; Soderholm, L.; Williams, C. W.; Blaudeau, J.-P.; Bursten, B. E. Neptunium redox speciation. *Radiochim. Acta* **2001**, *89*, 17–25, DOI: 10.1524/ract.2001.89.1.017.
- (S22) Ikeda-Ohno, A.; Hennig, C.; Rossberg, A.; Funke, H.; Scheinost, A. C.; Bernhard, G.; Yaita, T. Electrochemical and Complexation Behavior of Neptunium in Aqueous Perchlorate and Nitrate Solutions. *Inorg. Chem.* **2008**, *47*, 8294–8305, DOI: 10.1021/ic8009095.
- (S23) Denecke, M. A.; Dardenne, K.; Marquardt, C. M. Np(IV)/Np(V) valence determinations from Np  $\text{L}_3$  edge XANES/EXAFS. *Talanta* **2005**, *65*, 1008 – 1014, DOI: 10.1016/j.talanta.2004.08.034.

- (S24) Odoh, S. O.; Bylaska, E. J.; de Jong, W. A. Coordination and Hydrolysis of Plutonium Ions in Aqueous Solution Using Car-Parrinello Molecular Dynamics Free Energy Simulations. *J. Phys. Chem. A* **2013**, *117*, 12256–12267, DOI: 10.1021/jp4096248.
- (S25) Rothe, J.; Walther, C.; Denecke, M. A.; Fanghänel, T. XAFS and LIBD Investigation of the Formation and Structure of Colloidal Pu(IV) Hydrolysis Products. *Inorg. Chem.* **2004**, *43*, 4708–4718, DOI: 10.1021/ic049861p.
- (S26) Dardenne, K.; Seibert, A.; Denecke, M. A.; Marquardt, C. M. Plutonium(III, IV, VI) speciation in Gorleben groundwater using XAFS. *Radiochim. Acta* **2009**, *97*, 91–97.
- (S27) Antonio, M. R.; Williams, C. W.; Soderholm, L. Berkelium redox speciation. *Radiochim. Acta* **2002**, *90*, 851–856, DOI: 10.1524/ract.2002.90.12\_2002.851.
- (S28) Lutz, O. M. D.; Hofer, T. S.; Randolph, B. R.; Weiss, A. K. H.; Rode, B. M. A QMCF-MD Investigation of the Structure and Dynamics of  $\text{Ce}^{4+}$  in Aqueous Solution. *Inorg. Chem.* **2012**, *51*, 6746–6752, DOI: 10.1021/ic300385s.
- (S29) Sham, T. K. Electronic structure of hydrated  $\text{Ce}^{4+}$  ions in solution: An x-ray-absorption study. *Phys. Rev. B* **1989**, *40*, 6045–6051, DOI: 10.1103/PhysRevB.40.6045.
- (S30) Farkas, I.; Grenthe, I.; Bányai, I. The Rates and Mechanisms of Water Exchange of Actinide Aqua Ions: A Variable Temperature  $^{17}\text{O}$  NMR Study of  $\text{U}(\text{H}_2\text{O})_{10}^{4+}$ ,  $\text{UF}(\text{H}_2\text{O})_9^{3+}$ , and  $\text{Th}(\text{H}_2\text{O})_{10}^{4+}$ . *J. Phys. Chem. A* **2000**, *104*, 1201–1206, DOI: 10.1021/jp992934j.
- (S31) David, F. Thermodynamic properties of lanthanide and actinide ions in aqueous solution. *J. Less-Common Met.* **1986**, *121*, 27 – 42, DOI: 10.1016/0022-5088(86)90511-4, Proceedings of Actinides 85, Aix en Provence - Part I.

- (S32) David, F. H.; Vokhmin, V. Thermodynamic properties of some tri- and tetravalent actinide aquo ions. *New J. Chem.* **2003**, *27*, 1627–1632, DOI: 10.1039/B301272G.
- (S33) Shannon, R. D. Revised effective ionic radii and systematic studies of interatomic distances in halides and chalcogenides. *Acta Crystallogr. A* **1976**, *32*, 751–767, DOI: 10.1107/S0567739476001551.